

**PLASTIC OPTICAL FIBRE AS A SENSOR FOR  
TURBIDITY MEASUREMENT**

**by**

**STEPHENIE YEOH**

**Thesis submitted in fulfilment of the requirements  
for the degree of  
Master of Science**

**AUGUST 2015**

## ACKNOWLEDGEMENTS

First and foremost, my deepest gratitude goes to my supervisor, Professor Dr. Mohd Zubir bin Matjafri and co-supervisor, Dr. Kussay Nugamesh Mutter for their valuable advice and suggestions. I truly appreciate their continuous guidance and encouragements in molding me to accomplish a great research.

I would like to thank all the staffs and technicians at School of Physics, USM, for providing support, friendly services in a conducive environment. My sincere appreciation to the Institute Postgraduate Studies (IPS) for offering generous MyBrain scholarship program and USM Postgraduate Research Grant Scheme for the research funding. This research was supported by Universiti Sains Malaysia Research University Grant (1001/PFIZIK/811220) and Fundamental Research Grant (203/PFIZIK/6711349).

I would like to take this opportunity to thank Dr. Ahmad Fairuz Omar, lecturer of School of Physics, USM for providing scientific guidance and valuable research ideas that has contributed to the success in this research. My thankfulness also conveys to my fellow labmates Moo Yow Chong, Tan Chun Ho, Hwang Hsien Shiung, Tan Fuyi and Yeap Eong Chun for frequently exchanging fascinating ideas that fostered inspirations to my works.

Lastly, my appreciation goes to my beloved family and friends for their unconditional love and support that has given me internal strength and motivation in persevering towards the completion of research.

May the blessings and favours of God be upon all of you.

STEPHENIE YEOH, 2015

## TABLE OF CONTENTS

	<b>Page</b>
<b>ACKNOWLEDGEMENTS</b>	ii
<b>TABLE OF CONTENTS</b>	iii
<b>LIST OF TABLES</b>	vi
<b>LIST OF FIGURES</b>	vii
<b>LIST OF SYMBOLS AND ABBREVIATIONS</b>	xi
<b>LIST OF CONFERENCES AND PUBLICATIONS</b>	xiv
<b>ABSTRAK</b>	xv
<b>ABTRACT</b>	xvii
<b>CHAPTER 1 : INTRODUCTION</b>	1
1.1 Optical Wave Guide	1
1.2 Optical Fibre Sensor	3
1.3 Problem Statement	6
1.4 Scope of Study	6
1.5 Research Objectives	7
1.6 Thesis Layout	7
<b>CHAPTER 2 : LITERATURE REVIEW</b>	8
2.1 Introduction	8
2.2 Water Pollution in Developing Countries	8
2.3 Water Quality and Turbidity	9
2.3.1 Turbidity Standards and Units	10
2.3.2 Common Methods of Turbidity Measurement	11
2.3.3 Limitation	12
2.4 Geometrical Optics in Plastic Optical Fibre	13
2.4.1 Wave Equation	14
2.4.2 Fresnel Equation	15
2.4.3 Total Internal Reflection and Frustrated Total Internal Reflection	17
2.5 Evanescent Wave Fibre Optic Sensor	18
2.5.1 Evanescent Field in a Cylindrical Waveguide	19

2.5.2	Computing Number of Reflections	21
2.6	Optical Sensor Development and Design	22
2.7	Application of Evanescent Wave Optic Sensors	23
<b>CHAPTER 3 : METHODOLOGY</b>		29
3.1	Introduction	29
3.2	Research Design	29
3.3	Construction of Turbidity Probe	30
3.4	Sample Preparation	32
3.5	Experiment Setup	33
3.6	Turbidity Analysis	36
3.7	Preliminary Experiments and Characterisation of Turbidity Sensor	38
3.8	Turbidity Sensor Detection	40
3.8.1	Turbidity Measurement	40
3.8.2	Precision Detection	41
3.8.3	Real Water Sample	41
<b>CHAPTER 4 : RESULTS AND DISCUSSION</b>		42
4.1	Introduction	42
4.2	Modelling and Design of Fibre Sensor	42
4.3	Preliminary Experimental Analysis	52
4.3.1	Calibration Analysis	52
4.3.2	Basic Characterisation in Refractive Index	55
4.4	Turbidity Detection and Analysis	58
4.4.1	High Turbidity	59
4.4.2	Low Turbidity	65
4.4.3	Real Sample	71
4.6	Summary	77
<b>CHAPTER 5 : CONCLUSION AND RECOMMENDATION</b>		78
5.1	Conclusion	78
5.2	Future Works	79

**REFERENCES**

80

**APPENDICES**

85

## LIST OF TABLES

		<b>Page</b>
Table 3.1	Specification of QE65000 spectrometer	35
Table 4.1	Simulated results for different $\theta_o$ in the external medium of air and water	49

## LIST OF FIGURES

		<b>Page</b>
Figure 1.1	Electromagnetic spectrum	1
Figure 1.2	Optical fibre waveguide with core radius, $r_0$ surrounded by a cladding	2
Figure 1.3	Classification of optical fibre sensor and application areas	4
Figure 2.1	Reflectance and transmittance against incidence angle	17
Figure 2.2	Illustration of incident plane wave in optical fibre and exponentially decaying amplitude	19
Figure 2.3	Propagation of a meridional ray in a uniform straight core	21
Figure 2.4	Irradiance map displays show irradiance incident on the selected surface in watts per unit area and area in XY axis with millimeters scale	23
Figure 2.5	Single ray transmission interacts with particle	27
Figure 2.6	Reflectance against incident angle for various refractive indices of the external medium	27
Figure 2.7	Reflectance and transmittance against refractive index at $\theta_i = 63^\circ$	28
Figure 3.1	Flow diagram for research empirical analysis	30
Figure 3.2	Illustration of POF sensor in contact with random turbid particles	31
Figure 3.3	Configuration for POF sensor setup	33
Figure 3.4	TO-Can laser diode with typical parallel and perpendicular beam divergences of $10^\circ$ and $30^\circ$ respectively	34
Figure 3.5	Top view of QE65000 spectrometer	35
Figure 3.6	Spectra acquisition and signal-processing function in SpectraSuite software	36

Figure 3.7	Schematic fibre configuration of (a) reflective probe and (b) refractive probe showing evanescent wave propagates in opposing direction	39
Figure 4.1	Experiment modelled with simulation with dimension in reference to real experiment	43
Figure 4.2	Design of various bevel fibres with corresponding radius at the core surface, $r_o$ and their angles were measured in reference to the core axis in 3-dimension	44
Figure 4.3	Rays propagating out from the fibre with $n_i$ 1.492 into the cuvette containing air of $n_t = 1.000$ where $\theta_o$ is bevelled (a) perpendicular (b) $75^\circ$ (c) $60^\circ$ (d) $45^\circ$ (e) $30^\circ$ (f) $15^\circ$ to the surface to the core axis	45
Figure 4.4	Irradiance map traced from output detector screen of Figure 4.3 where $\theta_o$ is bevelled (a) perpendicular (b) $75^\circ$ (c) $60^\circ$ (d) $45^\circ$ (e) $30^\circ$ (f) $15^\circ$ to the surface to the core axis	46
Figure 4.5	Rays propagating out from the fibre with $n_i$ 1.492 into the cuvette containing water of $n_t$ 1.333 where $\theta_o$ is bevelled (a) perpendicular (b) $75^\circ$ (c) $60^\circ$ (d) $45^\circ$ (e) $30^\circ$ (f) $15^\circ$ to the surface to the core axis	47
Figure 4.6	Irradiance map traced from output detector screen of Figure 4.5 where $\theta_o$ is bevelled (a) perpendicular (b) $75^\circ$ (c) $60^\circ$ (d) $45^\circ$ (e) $30^\circ$ (f) $15^\circ$ to the surface to the core axis	48
Figure 4.7	Bevelled emitting and receiving fibre $\theta_o = 35^\circ$	50
Figure 4.8	Bevelled emitting and receiving fibre $\theta_o = 45^\circ$	50
Figure 4.9	Bevelled emitting and receiving fibre $\theta_o = 55^\circ$	51
Figure 4.10	Actual experiment setup for turbidity measurement	51
Figure 4.11	(a) Arroyo laser diode driver and (b) Thorlabs optical power and meter	53
Figure 4.12	Raw intensity signal of POF1, POF2 and POF3 immersed in distilled water as taken from QE65000 spectrometer measured against time	54
Figure 4.13	Normalised reference intensity of POF1, POF2 and POF3 in distilled water measured by QE65000 spectrometer against time	55

Figure 4.14	Rays paths undergoing refraction with external medium of $n_{t(i=1,2,3,...)}$ and TIR when $n_{t(i=c)}$ for (a) reflective and (b) refractive probe	56
Figure 4.15	Intensity distribution against the concentration of sucrose using reflective probe	56
Figure 4.16	Intensity distribution against the concentration of sucrose using refractive probe	57
Figure 4.17	Calibration linear graph of relative intensity against turbidity for POF1	60
Figure 4.18	Validation linear graph of relative intensity against turbidity for POF1 with RMSE 150.8317 NTU	60
Figure 4.19	Calibration linear graph of relative intensity against turbidity of POF2	61
Figure 4.20	Validation linear graph of relative intensity against turbidity of POF2 with RMSE 29.7893	62
Figure 4.21	Calibration linear graph of relative intensity against turbidity of POF3	63
Figure 4.22	Validation linear graph of relative intensity against turbidity of POF3 with RMSE 35.1283	63
Figure 4.23	Correlations of respective relative intensity in the range of 0 – 1010 NTU for POF1, POF2 and POF3 turbidity sensors	64
Figure 4.24	Calibration linear graph of relative intensity against turbidity for POF3	66
Figure 4.25	Validation linear graph of predicted turbidity against actual turbidity of POF3 with RMSE 2.1348 NTU	66
Figure 4.26	Calibration linear graph of relative intensity against turbidity for POF2	67
Figure 4.27	Validation linear graph of predicted turbidity against actual turbidity of POF2 with RMSE 2.3812 NTU	68
Figure 4.28	Calibration linear graph of relative intensity against turbidity for POF1	69
Figure 4.29	Validation linear graph of predicted turbidity against actual turbidity of POF1 with RMSE 132.2048 NTU	69

Figure 4.30	Linear slopes of relative intensity in the range 0 – 110 NTU for three turbidity sensors	70
Figure 4.31	Comparative turbidity in lake water samples determined by POF2 and turbidimeter	72
Figure 4.32	Comparative turbidity in river water samples determined by POF2 and turbidimeter	73
Figure 4.33	Comparative turbidity in sea water samples determined by POF2 and turbidimeter	73
Figure 4.34	Predicted turbidity by POF2 turbidity sensor in comparison with the actual turbidity of sample collected from Lake A	75
Figure 4.35	Predicted turbidity by POF2 turbidity sensor in comparison with the actual turbidity of sample collected from Lake B	75
Figure 4.36	Predicted turbidity by POF3 turbidity sensor in comparison with the actual turbidity of sample collected from Sea B	76
Figure 4.37	Predicted turbidity by POF3 turbidity sensor in comparison with the actual turbidity of sample collected from Lake A	76

## LIST OF SYMBOLS AND ABBREVIATION

Symbol/ Abbreviation	Caption
$r$	amplitude reflection coefficient
$r_{\parallel}$	amplitude reflection coefficient for parallel polarised light
$r_{\perp}$	amplitude reflection coefficient for perpendicular polarised light
$t_{\parallel}$	amplitude transmission coefficient for parallel polarised light
$t_{\perp}$	amplitude transmission coefficient for perpendicular polarised light
$\Gamma$	amplitude transmittance coefficient
$\theta_i$	angle of incidence
$\theta_z$	angle of ray with respect to z-axis
$I_{\text{avg}}$	average output intensity
$\theta_c$	critical angle
$I_n$	detected intensity
E	electric field
D	electric flux density
EM	electromagnetic
EPA	Environmental Protection Agency
$\beta$	evanescent absorption coefficient
EW	evanescent wave
f	flux density
$\nu$	frequency
FTIR	frustrated total internal reflection
IR	infrared
$I_o$	input intensity

$I_s$	intensity at saturation
L	length of fibre
H	magnetic field
B	magnetic flux density
$N_{max}$	maximum number of reflections per unit length
MMF	multimode fibre
NIR	near infrared
NTU	nephelometric turbidity unit
$N_{ref}$	number of reflections per unit length
$\theta_o$	oblique angle
$N_{conc}$	particle number concentration
$d_p$	penetration depth
POF	plastic optical fibre
PMMA	polymethyl methacrylate
$r_o$	radius of core fibre
R	reflectance
$P_R$	reflected power
RI	refractive index
$n_{clad}$	refractive index of clad
$n_{core}$	refractive index of core
$n_i$	refractive index of the incident medium
$n_t$	refractive index of the transmitted medium
$I_{relative}$	relative intensity
RMSE	root mean square error
$\mu_s$	scattering coefficient
C	scattering cross-section
SMF	single mode fibre

$c$	speed of light
$s$	standard deviation
$t$	time
TIR	total internal reflection
$T$	transmittance
$\tau$	turbidity
VIS-NIR	visible-near infrared
$V$	volume
$\emptyset$	volume fraction
$k$	wave vector
$\lambda$	wavelength of light

## LIST OF CONFERENCES AND PUBLICATIONS

1. Yeoh, S., Jafri, M.Z.M. and Omar, A.F., 2012. Revisiting the operating principles and application of interferometers, Photonics (ICP), 2012 IEEE 3rd International Conference on, pp. 103-106.

# **GENTIAN OPTIK PLASTIK SEBAGAI PENDERIA UNTUK MENGUKUR KEKERUHAN ABSTRAK**

Kekeruhan adalah penilaian terhadap penampilan optik yang disebabkan oleh zarah tidak larut dan bahan-bahan yang berwarna. Ia merupakan petunjuk penting kualiti air dalam ekosistem akuatik yang berkaitan dengan pencemaran di tasik, sungai dan kawasan pantai yang mengakibatkan masalah kesihatan persekitaran. Tujuan kajian ini adalah untuk mencipta penderia kekeruhan dengan menggunakan gentian optik plastik (POF) sebagai pengukur kekeruhan sampel air. Operasi pengesanan kekeruhan melibatkan pengukuran isyarat kembali yang disebabkan oleh serakan partikel-partikel terampai di dalam sampel air. Dalam kajian ini, pengukuran kekeruhan meliputi pemasangan inframerah (NIR) diod laser sebagai sumber cahaya NIR untuk dipancarkan ke dalam sampel akueus melalui POF dan gandingan pantulan balik isyarat kepada spektrometer. Sebelum eksperimen dimulakan, sistem optik telah disimulasi dengan pelbagai sudut kecondongan pada permukaan pengesanan untuk pengumpulan maklumat tentang ciri-ciri pergerakan cahaya dan penentuan parameter optimum dalam pembinaan penderia kekeruhan. Pengesan tersebut dimodelkan berdasarkan syarat-syarat pantulan dalam penuh (TIR) yang perlu dipatuhi di permukaan sudut gentian. Hasil daripada simulasi optik, POF digilap dengan sudut-sudut genting yang sesuai dan ditetap berdekatan antara satu sama lain untuk mengakses gelombang-gelombang evanesen (GE) di sempadan gentian. Sempadan tersebut adalah peka terhadap perubahan zarah dalam medium persekitaran dengan saiz sebesar panjang gelombang; seterusnya mengakibatkan modulasi keamatan. Modulasi keamatan diukur daripada interaksi perubahan fizikal

dalam indeks biasan (RI) dan kepekatan zarah terampai. Keputusan yang diperolehi telah dipersembahkan secara statistik dengan menjana persamaan terkalibrasi untuk setiap sudut dan analisis pengesanan dijalankan untuk memastikan kebolehpercayaan ramalan persamaan regresi. Pengesan kekeruhan yang paling sesuai diuji dengan sampel sebenar yang dikumpul dari tasik, sungai dan kawasan pantai untuk dibanding dengan ketepatan alat komersial dalam kompaun semula jadi. Pengesan kekeruhan dengan sudut serong  $45^\circ$  berupaya menjana regresi linear yang bagus dengan nilai  $R^2$  0.9954, RMSE 2.3812 NTU dan sisihan piawai sebanyak 0.5281% dengan keupayaan untuk mengukur kekeruhan sehingga 1000 NTU. Keputusan yang diperolehi daripada analisis sampel air menunjukkan bahawa penderia kekeruhan POF mampu menjana keputusan yang setara dengan mesin komersial dengan lingkungan pengesanan yang dinamik. Penderia yang dihasilkan merupakan satu pendekatan alternatif kepada penunjuk kualiti yang berkaitan dengan kesan alam sekitar.

# **PLASTIC OPTICAL FIBRE AS A SENSOR FOR TURBIDITY**

## **MEASUREMENT**

### **ABSTRACT**

Turbidity is an evaluation of optical appearance that was caused mainly by undissolved particles and coloured materials. It is an important indicator of water quality in aquatic ecosystem attributable to contamination in lake, river and coastal areas that could promote environmental health problems to the livings. The aim of this study is to develop a turbidity sensor using plastic optical fibre (POF) to perform measurement of turbidity in water samples. A turbidity sensor is operated by measuring the return signal that is caused by scattering of suspended particles present in turbid water. The designed experiment was conducted using a near infrared (NIR) laser diode as light source to emit NIR light into aqueous samples via POFs and to couple the back reflected signal to the spectrometer. Prior to the execution of the experiment, the optical system was simulated with various angles of inclined surface to collect information on light propagation behaviour and to determine optimum parameters in developing turbidity sensor. The sensor was modelled for the conditions of total internal reflection (TIR) to be met at the surface of the angled tip. Subsequently, the determined oblique angles from the optical simulation are polished and placed in close proximity to one another to tap evanescent wave (EW) at the boundary. The EW localised at the polished surface is sensitive to changes in the surroundings particles of size in its wavelength; thus resulting in an intensity modulation. The resulting intensity modulation was measured from the interaction of external change in refractive index (RI) and concentration of suspended particles. The results obtained were presented statistically by generating calibration equations

for each developed angle and validation analyses were conducted to ensure the reliability of the predicted regression equations. The fitting turbidity sensor is tested with real samples that are collected from lake, river and coastal areas to match its accuracy with commercial apparatus in natural compounds. The turbidity sensor with oblique angle  $45^\circ$  was able to generate reliable linear regression with  $R^2$  of 0.9954, RMSE 2.3812 NTU and standard deviation of 0.5281 % with an ability to measure turbidity up to 1000 NTU. The results obtained from real samples analysis show that the developed POF turbidity sensor produced comparable results to the commercial device with a dynamic range of detection. The developed sensor is an alternative approach to quality indicator related to environmental effects.

# CHAPTER ONE

## INTRODUCTION

### 1.1 Optical Wave Guide

Electromagnetic (EM) waves consist of waves of energy associated with electric and magnetic components resulting from vibrating electric charge which is capable of travelling and transporting energy through a vacuum. EM is divided into a range of spectrum according to wavelength called EM spectrum as shown in Figure 1.1. EM wave is a uniform emission until it interacts with matter.

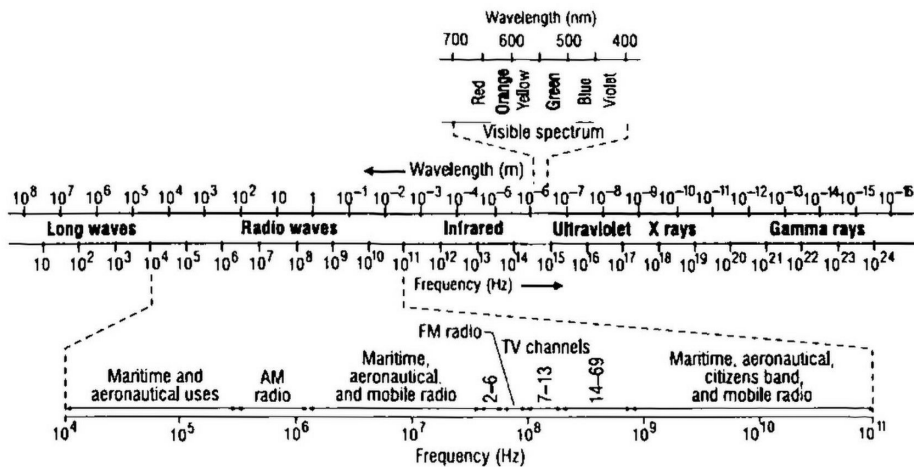


Figure 1.1 Electromagnetic spectrum (Roychoudhuri, 2008).

Light could exhibit absorption, scattering reflection or refraction when it encounters a medium. Absorption is a transfer of energy from the EM wave to the atoms or molecules of the medium causing molecule to excite vibrations or rotations and generate thermal energy. Scattering is the physical process that occurs when light interacts with matter forcing redirection of light propagation. Reflection involves a change in direction of waves when they bounce off a barrier. Whereas, refraction of waves involves a change in the direction of waves as they pass from one medium to

another. Refraction, or the bending of the path of the waves, depends on the change in speed and the wavelength of light (Jenkins and White, 1976).

In order to carry light beam signal, the EM wave is guided by a medium called an optical wave guide. Figure 1.2 illustrates an optical fibre which typically acts as a waveguide. It is made of extruded glass (silica) or plastic and its efficiency has replaced the conventional copper wire systems. Fibres that allow propagation of many modes within the core are known as multimode fibres (MMFs). Another type of mode coupling is the single mode fibre (SMF) which allows propagation of only one transverse EM mode, while other modes are attenuated by leakage or absorption (Powers, 1997). Optical fibre is an application of successive total internal reflections (TIRs) which makes use of flexible glass or plastic to confine light in order to travel from one place to another. Optical fibre is capable of carrying a huge amount of information in high efficiency brings various contributions in scientific advances especially in technology associated with the optoelectronic and fibre optic communications industry.

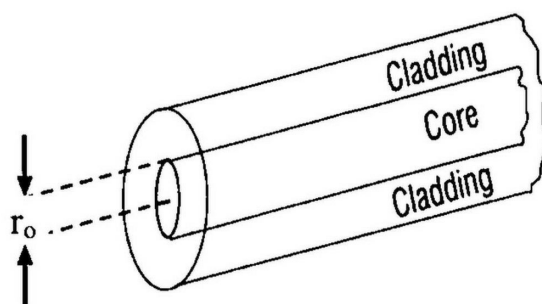


Figure 1.2 Optical fibre waveguide with core radius,  $r_0$  surrounded by a cladding.

Optical fibre consists of a transparent core that is surrounded by a lower index of refraction material, cladding. The cladding executes such functions as preventing loss of light from core into the surrounding air, decreasing scattering loss at the surface

of the core, protecting the fibre from absorbing the surface contaminants and adding mechanical strength. The combination may be surrounded by a plastic jacket to prevent mechanical damage. Due to the smaller index of refraction of the cladding than that of the core, light travelling at an angle of incidence,  $\theta_i$  in the core that exceeds the critical angle,  $\theta_c$  experiences TIR if it arrives at the core-cladding interface. In this case, light repeatedly bounced along the core of the optical fibre, losing very little of its intensity as it travels. The refractive index (RI) profile of the core-cladding interface may either be abrupt, in step-index fibre, or a gradual decrease with radial distance, in graded-index fibre (Serway and Jewett, 2014).

## **1.2 Optical Fibre Sensor**

Fibre optic sensor technology has developed enormously since the early 1970s. Being excellent in monitoring a wide range of environmental parameters, they soon replaced the conventional sensors. Primary advantages of fibre optics sensors include compactness, light weight, immunity to EM interference, high sensitivity and economical fabrication. In the market place, optical fibre sensor products are expanding in sensing and measuring physical parameters such as linear and angular displacement, acceleration, electric and magnetic field, temperature, pressure, vibration, strain, humidity and liquid RI (Udd, 2011).

The classification of optical fibre sensor and their applications are summarised in Figure 1.3. Fibre optic sensors are broadly classified into intrinsic and extrinsic sensors. In the former, the sensing occurs within the optical fibre itself. The properties of the guided light alter the properties of the optical fibre. While in the latter, the optical fibre is used to deliver signal, usually to and from a sensing element where the light

beam is influenced by the measured medium. It has an advantage to be specially designed to maximise the modulation of the light signal, but suffers a resultant loss of optical power and the danger of contamination of optical surfaces.

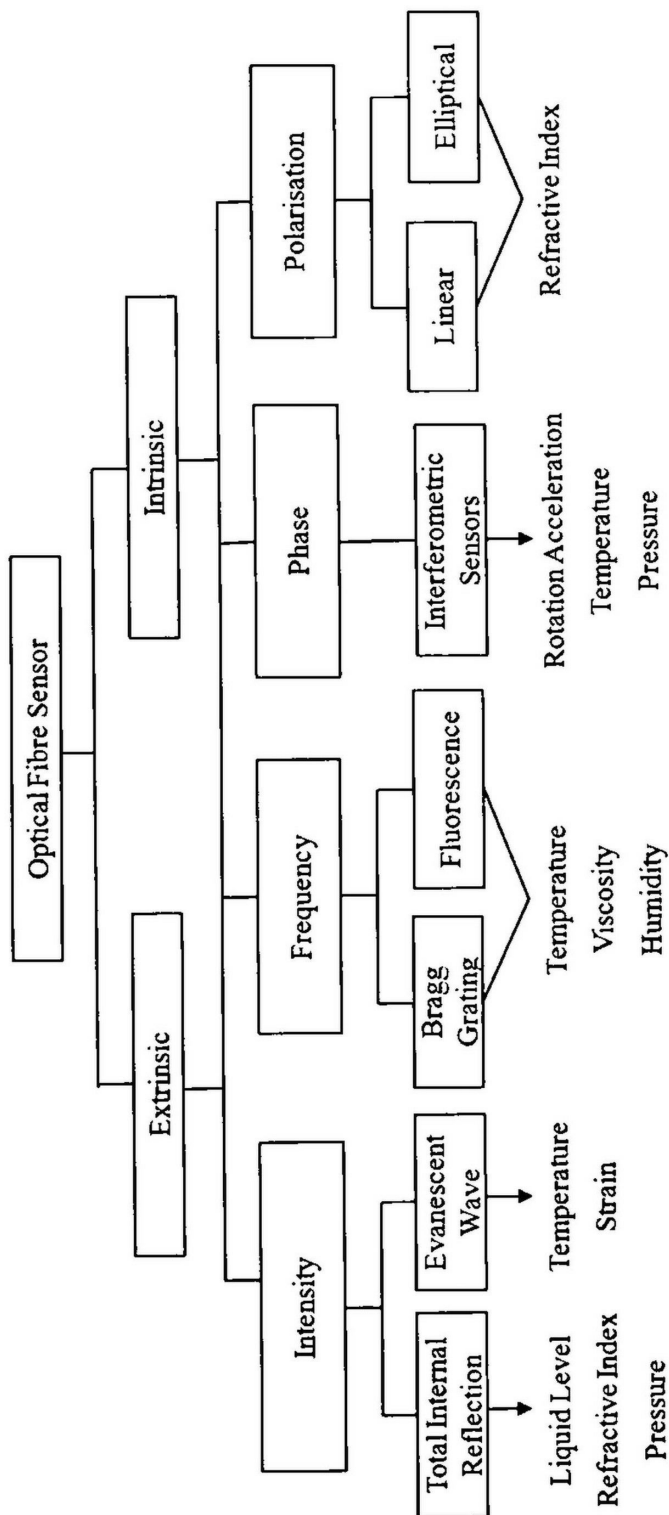


Figure 1.3 Classification of optical fibre sensor and application areas.

Plastic optical fibre (POF) shares the advantages of glass optical fibre in terms of its insensitivity to EM interference, small size and weight, low cost and potential capability of carrying information at high rates. Besides, POF has larger core radii and higher numerical aperture than glass fibres that easily facilitates efficient coupling to optical sources. Recent advances in polymer material leads to improvement of POF in terms of high bandwidth, low loss, attenuation characteristics and increased temperature tolerance. The sensing core material of POF is polymethyl methacrylate (PMMA). The satisfactory transmission level over a reasonable length takes advantage of the enhanced flexibility and durability that plastic gives over silica (Roychoudhuri, 2008).

The major characteristic of optical fibres is that it extracts optical information transmission of intensity, phase, frequency, polarization and spectral content depending on application areas. Among the most widely studied sensor types are evanescent wave (EW) sensor, fibre-grating sensor and interferometric sensor. Optical multimode plastic bundle fibre is typically used as a probe for intensity-based fibre sensors, interferometry-based and intensity-based sensors (Yu et al., 2008). Generally, intensity modulation of fibre optic sensors is achieved from the mechanisms of misalignment losses in MMF, absorption, scattering light losses or evanescent coupling to another fibre. Thereby, extensive research which exploits the exponentially decaying evanescent field in sensing the lower index region of turbidity and fluorescence were done previously (Cong et al., 2011; Gupta, 2006; Nath and Anand, 1998). This technique, in particular, is one that continues to expand with the wide range of applications in optical sensing which can be particularly important for simple, yet effective sensor systems in mass miniature production. The conventional

bulk optics method is unsuitable for measurement of highly absorbing or scattering media. EW sensors perform accurate signal acquisition of tested samples due to the short effective path length of evanescent field (Grattan and Meggitt, 1999).

### **1.3 Problems Statement**

Turbidity, an optical property of water that causes light to be scattered or absorbed, is one complex parameter to measure. The murky and opaque water is caused by undissolved particles and coloured materials, and they can be a subjective measurement. Turbidity plays an important role from domestic usage of water and control in agriculture quality to monitor the pollution and danger it cause to our health in long term. However, monitoring the water quality requires expensive and time consuming apparatus due to the need of sample preparation as well as repetitive and continuous measurement (Gibs et al., 2000). The existing measurement methods involve the effects of background colour, interference and scattering of suspended particles that limits the accuracy of collected signals in a certain range (Ji and Chen, 2014). Simple setup and economic instruments that provide wide measuring range and sensitive in distinguishing minor resolution changes are crucial in environmental applications. Imparting evanescent wave greatly increases sensing efficiency and the proposed sensor has potential to replace conventional sensors.

### **1.4 Scope of Study**

This work mainly focuses on study of TIR and EW to build a sensor to determine the turbidity of an aqueous solution. The structure of the fibre probe is first simulated to aid in obtaining few experimental parameters. The turbidity of these solutions are measured and compared with a turbidity instrument, Turbichex. In the final stage of

this study, analysis and regression curves are collected for calculation of turbidity in solution and the test of turbidity sensor with real samples. The spectrometer, QE65000 used in this study measures intensity in unit counts.

### **1.5 Research Objectives**

The objectives of this study are as follow:

1. To examine total internal reflection by changing incident angle of fibre to be close to the critical angle to tap evanescent wave in optical simulation.
2. To design turbidity sensor and determine the turbidity with different concentrations of standard solution.
3. To validate the turbidity sensor with commercial method for real water samples.

### **1.6 Thesis Layout**

This thesis consists of five chapters. First chapter provides an overview of this study, problems statements, scope of study and research objectives. Literature reviews will be covered in chapter two which include some current works by researcher and basic theory such as EM waves, TIR and simulated theory. Chapter three describes the instruments and method used in this study. Chapter four presents the results of the research with discussion and analysed results. Chapter five summarises all the output and result of this research with recommendation for future study. Finally, the evanescent wave theoretical derivation and results will be included in the appendix.

## **CHAPTER TWO**

### **LITERATURE REVIEW**

#### **2.1 Introduction**

This chapter introduces theoretical models of fibre optic evanescent sensors built using both EM field theory and geometric optics. Basic optical concepts and similar previous studies of intensity modulated evanescent sensors were discussed to help understanding the concept and design in this study.

#### **2.2 Water Pollution in Developing Countries**

With rapid industrial growth, the severe consequences of industrial pollution in environmental health problems have caught the global attention (Schwarzenbach et al., 2010). Waste pollution is an inevitable by-product of agricultural activities, industrial discharge, municipal landfill, tourism development and coastal reclamation. The industrial wastewater discharged into rivers, lakes and coastal areas can cause collateral damage to the aquatic ecosystem. The developing countries were targeted as disposal or recovery grounds by the developed ones (Kummer, 1995). Most developing countries lack of funds and sufficient knowledge to handle these wastes in an environmentally sound manner causing the increasing rate of industrial wastewater in developing countries are significantly higher than those in developed countries (Rogers and Secretariat, 2000). The contamination was reported to account death of more than 14000 people daily and predicted potential hazards to the population (DOE, 2010). The water pollution has to be monitored and controlled to sustain the ecological processes.

### **2.3 Water Quality and Turbidity**

Water quality is defined as the physical characteristic of water and optical property that causes light being scattered by suspended particles in the water sample. Turbidity is the measure for the suitability of a particular water system for human consumption and the key to sustaining water content from pollution. Simply, high turbidity measurements indicate higher chances in the presence of disease-causing organisms in natural water. Turbidity measurement is an important physical parameter for quality assessment of liquids before proceeding to water treatment. Turbidity is caused by suspended matter that includes organic matter, floating debris, algae, air bubbles and soluble water coloured organic compounds (Omar and MatJafri, 2013). Among the parameters that may affect the turbidity measurements comprise of the suspended particles' properties such as particle size, configuration, colour and refractive index that which affects the spatial distribution of the scattered light intensity around the particle (Johnson et al., 1997).

Turbidity is an important water quality indicator that measures the scattering and absorption effect between suspended solids and light; higher intensity of scattered light implies higher turbidity. They are loose particles of sand, clay, silt, mud, faecal matter and organic particles. Although turbidity is not an inherent property of water, the recognition of turbidity as an ecologically important parameter has increased over the past decade (Davies-Colley and Smith, 2001). Hence, there is a growing demand for high-quality and objective turbidity measurements. The turbidity of Malaysia's river water quality standard is 50 NTU (DOE, 2010). The acceptable raw water quality criteria is 1000 NTU and treated water of 5 NTU (MOH, 2010). Over the years, relatively inexpensive yet sophisticated instruments have been developed that allow

nearly continuous monitoring and data logging of turbidity in natural waters. Numerous studies shows that change in turbidity often indicate issues in aquatic ecosystem, such as development of an algal bloom on a lake or a steady increase in suspended sediment in a river (Davies-Colley and Smith, 2001; Gibs et al., 2000). High turbidity levels decrease light penetration from reaching the submerged aquatic plants which acts as a common food supply. Therefore, designing new methods that allows continuous monitoring and real time measurement in identifying contaminated areas for further analytical examination is essential in sustaining a pollution-free environment.

### **2.3.1 Turbidity Standards and Units**

Turbidity being a qualitative parameter for water has traceability to a primary standard that allows quantitative methods to be developed. A frame of reference to calibrate the units was first established in 1926 when formazin was proposed by Kingsbury and Clark (1926). The measuring units were renamed to formazin turbidity units (FTU). Formazin, a stable synthetic material, is the polymerisation of hexamethylenetetramine and hydrazine sulfate in water. Its physical characteristics lead to consistency in standards formulation to improve greatly and it was accepted as the primary standard worldwide. With median particle size of 1.5  $\mu\text{m}$  and the standard deviation of size is 0.6  $\mu\text{m}$ , formazin has relatively large particles that is suitable to calibrate the instrument of larger particles. Nowadays, most turbidity readings are expressed in nephelometric turbidity unit (NTU) (Sadar, 2004).

### **2.3.2 Common Methods of Turbidity Measurement**

Concentration of total suspended particles in water can be detected by various types of optical sensing techniques depending on the turbidity range to meet the criterion set by Environmental Protection Agency (EPA, 1999). In general, turbidity assessment performed in the laboratory compliant to the requirements ISO 7027 were designed according to ratiometric, nephelometric (single beam), absorptometric (transmittance), surface-scatter, backscatter and multiple-beam (ISO, 1999).

Portable turbidimeter design for turbidity determination was based on the Jackson candle turbidimeter (Whipple and Jackson, 1900). This instrument is essentially the inverse measure of the depth of the sample in the tube needed to completely diffuse a uniform glow of candle (AWWA, 2011). The preferred basic designs for turbidity measurement are nephelometers and absorptometers. Nephelometer measures low turbidity in the unit Nephelometric Turbidity Units (NTU) as reported (EPA, 1999). It measures the intensity of light scattered by suspended particles at 90 degree from the light source. Nephelometric principle compares the light scattered due to a sample with the light scattered by a standard reference suspension (Rice et al., 2012). Conversely, the absorptometer measures the intensity of light beam that is transmitted through the sample by a photodetector in line with the light source. Another type of turbidimeter that is suitable for high turbidity measurement uses backscatter detection. This design measures the transmitted light reflected back to the detector in the direction of the incident light source and it is proportional to the particle concentrations in the sample.

Turbidity employed in field work can be measured through surface water clarity method using Secchi disk or a transparency testing tube. A Secchi disk is a black and white disk that is lowered into the water to measure the depth at which it vanishes from sight to indicate transparency of water (Spellman, 2013). The technique used in turbidity tube is analogous to Secchi disk; it is suitable for shallow pure water.

Common on-line instruments that offers in-situ monitoring of current include turbidity sensor for measurement in streams, rivers, lakes and oceans (Anderson, 2005). A turbidity sensor operates by detecting the light that scatters off the suspended particles present in the water. POF has the advantage of high transmission in the visible-near infrared (VIS-NIR) range, high mechanical stability and resistance to chemical degradation. Turbidity sensors also uses nephelometric technology (Ji and Chen, 2014) and backscatter instruments (Shenoy, 2014).

### **2.3.3 Limitation**

As described in the previous reports (Omar and MatJafri, 2009), there are still a lack of turbidimeters that have capability to cover a wide range of measurement and provide high sensitivity. Nephelometric method allow a greater measurement range with precision of turbidity. However, this method is unsuitable for streams with strongly absorbing or scattering suspended solids. Particulate, such as coal dust, has limited reflective abilities and tends to absorb light and thus it will produce false results. The absorptometer method works great in the presence of larger particles but this method do not measure the true turbidity in NTU. Whereas, the backscatter method has power loss limitation due to the influence of weak light sources when multiple scattering

between the suspended particles is triggered. Thus, this technique is less popular for low level turbidity monitoring because it has inherent poor sensitivity at these levels.

Electronic turbidity readings can deviate from the actual turbidity value due to the transmission sensitivity to imperfections and scratches in the glass measuring cell. Using portable turbidimeter for field work requires extra expenses in logistic and complications in risking damage to the glass measuring cell. Grab sampling technique limits to the samples available on the surface of the system. The operating time taken for data collection is considerably longer for averaging.

The current commercial techniques are unsuitable to perform continuous monitoring of water quality for sewer system due to its restricted space and an inconvenience for process applications in a separate laboratory (Hur et al., 2010). Most commercial sensors that provides high accuracy were built with expensive components with complex setup and unsuitable for high turbidity measurement. Therefore, there is a requirement for a simple, inexpensive, in-situ and alarm level water pollution measurement.

#### **2.4 Geometrical Optics in Plastic Optical Fibre**

In order to give an analytic description of the phenomena in media, it is necessary to gain understanding of the mechanism within waveguide and proper visualisation of the optical propagation by solving the basic EM wave equation for incident evanescent plane waves. This section examines EW for purely elastic planar structure models.

### 2.4.1 Wave Equation

Maxwell described the basis study of EM wave propagation in the form of integral equations valid for all geometric configurations. The solutions of Maxwell equations in a uniform, isotropic, non-conducting, charge-free and non-dispersive optical medium are written in terms of electric field,  $E$ , magnetic field,  $H$ , electric flux, density,  $D$ , and magnetic flux density,  $B$  as expressed in equations (2.1) – (2.4) (Maxwell, 1865).

$$\nabla \times \mathbf{E} = -\frac{\partial \mathbf{B}}{\partial t} \quad (2.1)$$

$$\nabla \times \mathbf{H} = \frac{\partial \mathbf{D}}{\partial t} \quad (2.2)$$

$$\nabla \cdot \mathbf{D} = \rho \quad (2.3)$$

$$\nabla \cdot \mathbf{B} = 0 \quad (2.4)$$

Where  $\rho$  is flux density and  $t$  is time.

For a medium in vacuum, Maxwell's equation predicted the existence of EM waves that can transport energy and travel with the speed of light  $c$ . Coupling between the two fields leads to the generation of EM waves. Applying Maxwell's equation to the classical wave equation in equation (2.5), it is derived in the form of a uniform sinusoidal-plane wave in equation (2.6).

$$\frac{1}{c^2} \frac{\partial^2 \mathbf{E}}{\partial t^2} - \nabla^2 \mathbf{E} = 0 \quad (2.5)$$

$$\vec{\mathbf{E}}_{0i} \exp [i(\vec{\mathbf{k}}_i \cdot \vec{\mathbf{r}} - \omega_i t)] = \vec{\mathbf{E}}_{0t} \exp [i(\vec{\mathbf{k}}_t \cdot \vec{\mathbf{r}} - \omega_i t)] + \vec{\mathbf{E}}_{0r} \exp [i(\vec{\mathbf{k}}_r \cdot \vec{\mathbf{r}} - \omega_i t)] \quad (2.6)$$

Where  $\mathbf{E}_{0i}$ ,  $\mathbf{E}_{0t}$  and  $\mathbf{E}_{0r}$  are the incident, transmitted and reflected electric field components,  $k_i$ ,  $k_t$  and  $k_r$  are their propagation vectors,  $\mathbf{r}$  states the direction of their tangential components and  $\omega_i$  is the angular frequency.

### 2.4.2 Fresnel Equations

The Fresnel equations described the relationship between reflection and refraction of light at uniform plane interface travelled into a medium of differing refractive indices at an angle determine by Snell's Law. The relationship between the angles of incident, reflected and refracted rays are governed by Snell's law. Snell's law, also known as Descarte's law or the law of refraction states that the ratio of the sines of the angle of incidence,  $\theta_i$  and angle of refraction,  $\theta_t$  is equivalent to the ratio of phase velocities in the two media, or equivalent to the reciprocal of the ratio of the indices of refraction as represented in equation (2.7) (Serway and Jewett, 2014).

$$n_i \sin \theta_i = n_t \sin \theta_t \quad (2.7)$$

Where  $n_i$  is the refractive index of the incident medium and  $n_t$  is the refractive index of the transmitted medium.

Amplitude coefficients of reflection and transmission were developed from Fresnel equations to compute the reflected and transmitted power relative to the incident power quantitatively. The generalised Fresnel reflection coefficient,  $r$  and transmission coefficient,  $\Gamma$  are able to study EM field configuration applicable to any linear, isotropic and homogenous media. Since the amplitude is dependent on state of polarisation of the incident ray, the direction propagation is to be considered. The media are assumed to be non-magnetic and non-absorbing in order to obtain mathematical descriptions in equation (2.8) to equation (2.11).

$$r_{\perp} = \left( \frac{E_{0r}}{E_{0i}} \right)_{\perp} = \frac{n_i \cos \theta_i - n_t \cos \theta_t}{n_i \cos \theta_i + n_t \cos \theta_t} = \frac{\sin (\theta_i - \theta_t)}{\sin (\theta_i + \theta_t)} \quad (2.8)$$

$$t_{\perp} = \left( \frac{E_{0t}}{E_{0i}} \right)_{\perp} = \frac{2n_i \cos \theta_i}{n_i \cos \theta_i + n_t \cos \theta_t} = \frac{2 \sin \theta_t \cos \theta_i}{\sin (\theta_i + \theta_t)} \quad (2.9)$$

$$r_{\parallel} = \left( \frac{E_{0r}}{E_{0i}} \right)_{\parallel} = \frac{n_t \cos \theta_i - n_i \cos \theta_t}{n_i \cos \theta_t + n_t \cos \theta_i} = \frac{\tan (\theta_i - \theta_t)}{\tan (\theta_i + \theta_t)} \quad (2.10)$$

$$t_{\parallel} = \left( \frac{E_{0t}}{E_{0i}} \right)_{\parallel} = \frac{2n_i \cos \theta_i}{n_i \cos \theta_t + n_t \cos \theta_i} = \frac{2 \sin \theta_t \cos \theta_i}{\sin (\theta_i + \theta_t) \cos (\theta_i - \theta_t)} \quad (2.11)$$

Where  $E_{\perp}$  and  $E_{\parallel}$  is the electric field vectors perpendicular and parallel to the plane of incidence. The polarisation in transverse electric field direction of amplitude reflection coefficient,  $r$  is denoted as  $r_{\perp}$  and amplitude transmission coefficient,  $\Gamma$  as  $t_{\perp}$ . The polarisation in transverse magnetic field direction of amplitude reflection coefficient,  $r$  is denoted as  $r_{\parallel}$  and amplitude transmission coefficient,  $\Gamma$  as  $t_{\parallel}$ . The difference in both amplitude coefficients,  $\Gamma - r = 1$  over the entire range of angles is a direct consequence of Maxwell's continuity conditions.

Reflectance,  $R$  is the ratio of the reflected power to the incident power as stated in equation (2.12) while for transmittance,  $T$  which is the ratio of the transmitted power to the incident power was stated equation (2.14). Equation (2.13) and equation (2.15) showed the relationship with their amplitude coefficients respectively. The reflection coefficient increases sharply when  $\theta_i$  draws closer to  $\theta_c$ . It can be shown simply by conservation of energy, the summation of  $R$  and  $T$  is equal to one which can be deduced from Figure 2.1 below. As a result, equation (2.16) is computed.

$$R = \frac{I_r \cos \theta_r}{I_i \cos \theta_i} = \frac{I_r}{I_i} \quad (2.12)$$

$$R = r^2 \quad (2.13)$$

$$T = \frac{I_t \cos \theta_t}{I_i \cos \theta_i} \quad (2.14)$$

$$T = \left( \frac{n_t \cos \theta_t}{n_i \cos \theta_i} \right) t^2 \quad (2.15)$$

$$r^2 + \Gamma^2 \left( \frac{n_t \cos \theta_t}{n_i \cos \theta_i} \right) = 1 \quad (2.16)$$

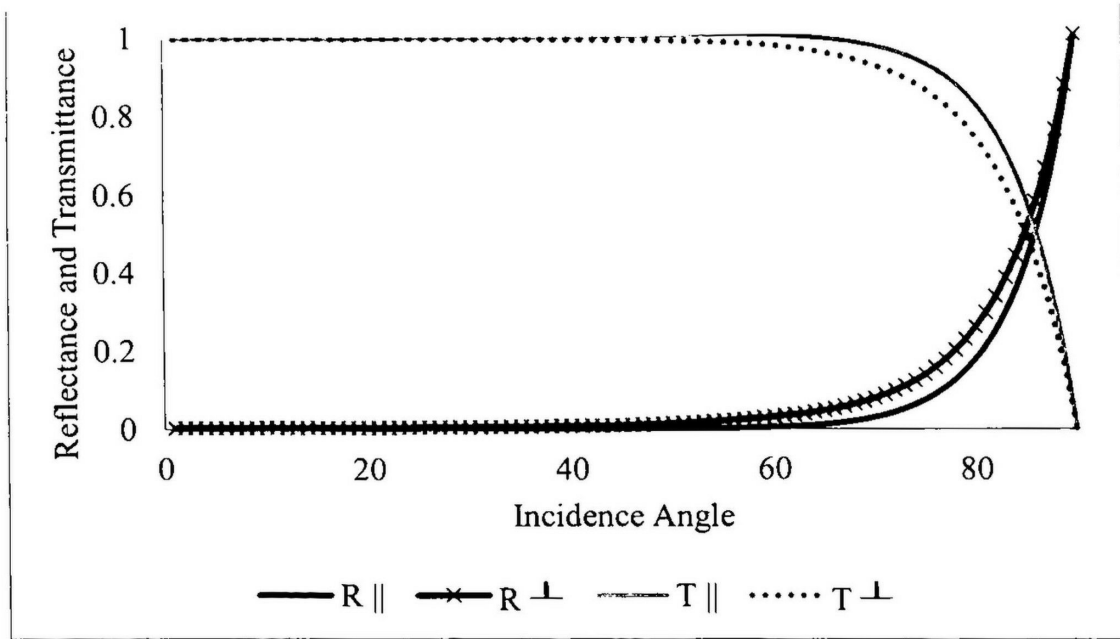


Figure 2.1 Reflectance and transmittance against incidence angle.

### 2.4.3 Total Internal Reflection and Frustrated Total Internal Reflection

TIR being an optical phenomenon utilised in fibre optics occurs when a ray that propagates from a less dense interface with  $\theta_i$  equal to or greater than  $\theta_c$ . Transmitted ray gradually approaches tangency with the boundary as  $\theta_i$  nears to  $\theta_c$  until all the light is reflected back into the plane of incident medium. Since the incident and reflected waves are in the same plane, equation (2.7) is reduced to equation (2.17) (Serway and Jewett, 2014).

$$\sin \theta_c = \frac{n_t}{n_i} \quad (2.17)$$

The field configuration at the higher refractive index incident medium could be significantly altered by introducing an object at vicinity. The process where TIR is frustrated thereby permitting energy to flow into the second medium is known as

frustrated total internal reflection, FTIR. The frustrated field excites other form of EM radiation and becomes propagating waves that transmits energy to retrieve near-field information in several wavelengths across the medium (Zhu et al., 1986). The energy transmission was shown in a simple demonstration of FTIR in a double prism (Rabiya et al., 2013).

## **2.5 Evanescent Wave Fibre Optic Sensor**

Coupling of EM light source into MMF based on intensity modulation are widely exploited for physical and chemical parameters sensing. The particularity of evanescent field in its exponentially decaying EM field amplitude in the fibre cladding has grown rapidly in terms of its involvement and contribution in sensitive and quick response in interaction with measurand. Recently, such working mechanism is still actively fabricated in numerous sensors configuration to detect concentration (Botero-Cadavid et al., 2013; Dutt-Ballerstadt et al., 2014), refractive index (Harun et al., 2013) and displacement (Berkovic and Shafir, 2012; Vallan et al., 2012).

The advantages of an optical fibre that include low loss in remote access, high bandwidth, chemical inertness, resistant to EM interference, nonconductive and susceptible to temperature fluctuation are suitable for on-site direct sensing. The breakthrough in optical fibre spectroscopy research in guided light through a thin flexible dielectric waveguide with low loss characteristics and larger information capacity has replaced most conventional techniques (Borecki, 2007; Chong et al., 2013; Kao and Hockham, 1966).

### 2.5.1 Evanescent Field in a Cylindrical Waveguide

An EW is a near-field standing wave with an intensity that exhibits exponential decay with distance from the boundary at which the wave was formed. Figure 2.2 illustrates a plane wave propagating in the z-direction of an optical fibre.

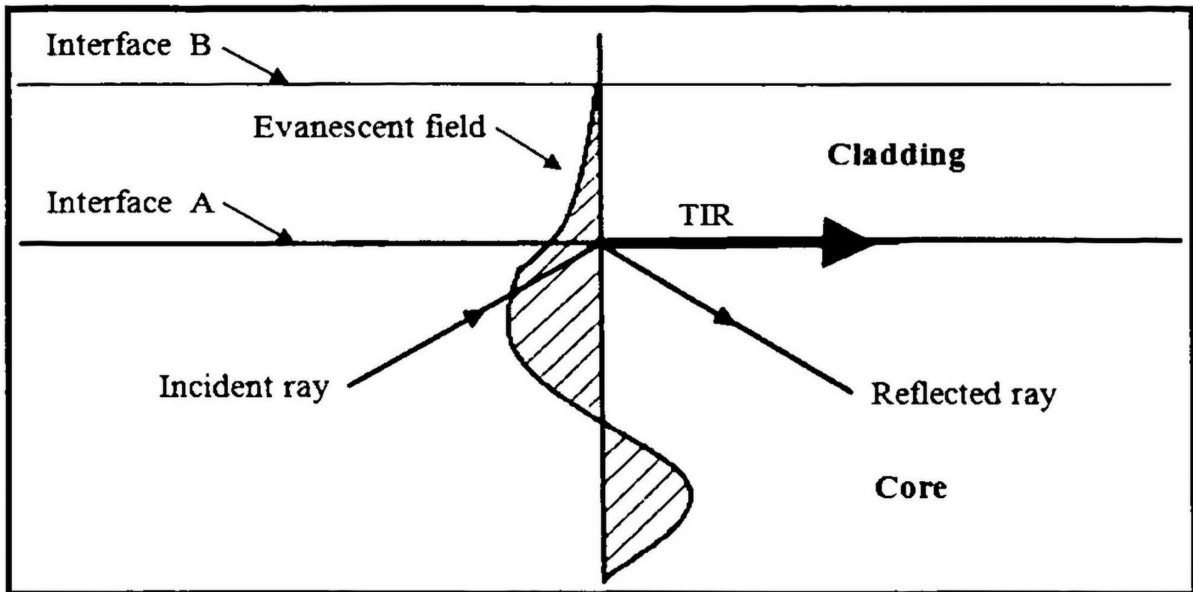


Figure 2.2 Illustration of incident plane wave in optical fibre and exponentially decaying amplitude.

EWs are an EM field formed at the boundary when light waves are reflected off an interface at a sufficiently shallow angle, called the  $\theta_c$ , whereby TIR occurs. The evanescent field arises from the interference between the electric fields of the incoming and reflected rays. The existence of the EW is essential to satisfy the continuity conditions for electric field because the field in lower refractive index cladding cannot vanish abruptly. The energy flow of this EW is parallel to the surface of the core and in the same direction as the main flow of energy within the core. The amplitude is in the direction perpendicular to its surface of generation and the incident frequency is retained.

To satisfy boundary conditions, there must be transmitted wave with an identical frequency to the incident light. Therefore, it is expected that there is a small amount of penetration of the reflected light across the interface, which then propagates parallel to the surface of the lower RI medium. The EM field amplitude typically decays exponentially with distance less than 100 nm on the interface of the second medium. In the situation of TIR, the resultant transmitted electric field along the unclad length,  $z$  is solved from Maxwell's equation in equation (2.6) and expressed in equation (2.18) (Hecht, 2002).

$$\vec{E}_t = \vec{E}_{0t} \exp[-\beta z] \exp i \left[ \left( \frac{k_t x n_i \sin \theta_i}{n_t} - \omega t \right) \right] \quad (2.18)$$

Where  $\beta$  is the evanescent absorption coefficient.

The penetration depth of the evanescent field denoted as  $d_p$  is the perpendicular distance from the core-cladding interface at which the electric field amplitude decreases to  $1/e$  of its initial value. The penetration depth is related to wavelength  $\lambda$ , refractive indices and  $\theta_i$  as given by equation (2.19). The evanescent power residing in the cladding,  $P_{clad}$  computed as a ratio to the total power,  $P_{total}$  is as shown in equation (2.20).

$$d_p = \frac{\lambda/n_t}{2\pi \sqrt{\left(\frac{n_i}{n_t \sin \theta_i}\right)^2 - 1}} = \frac{\lambda}{2\pi n_i \sqrt{(\sin^2 \theta_i - \sin^2 \theta_c)}} \quad (2.19)$$

$$\frac{P_{clad}}{P_{total}} = \frac{4\sqrt{2}}{3} \frac{\lambda}{2\pi r_o \sqrt{n_i^2 - n_t^2}} \quad (2.20)$$

## 2.5.2 Computing Number of Reflections

Evanescent field exists at the end of the fibre depends on the number of TIRs occurs within the fibre length and ray transmission (Okamoto, 2006). Evanescent absorption coefficient  $\beta$  is given by:

$$\beta = N_{ref}T \quad (2.21)$$

Where  $N_{ref}$  is the number of reflections per unit length and  $T$  is the Fresnel transmission coefficient.

Figure 2.3 shows the guided incident light by TIR in a conventional MMF with radius of core,  $r_0$  segmented to reflection points in distance  $l$ . The number of TIR per unit length,  $N_{ref}$  for a meridional ray is computed in the following equation (2.22). The number of reflections is dependent on its  $\theta_i$ , length of fibre,  $L$  numerical aperture, NA and inversely proportional to  $r_0$  (Gupta, 2006).

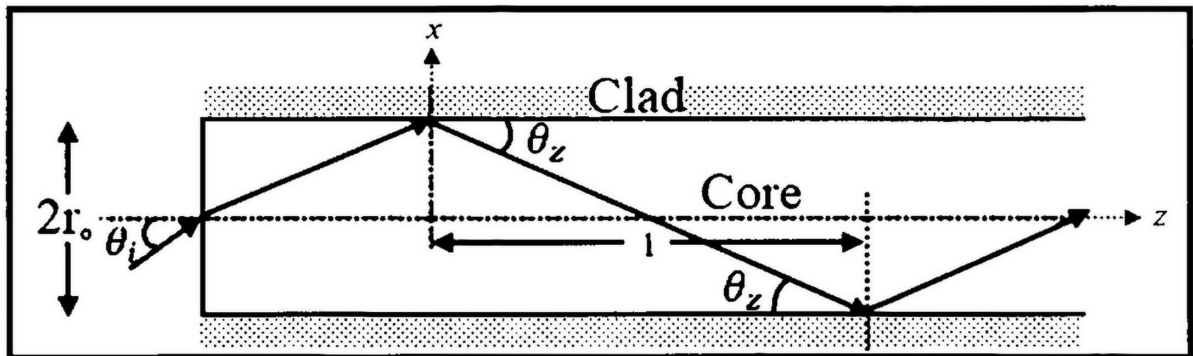


Figure 2.3 Propagation of a meridional ray in a uniform straight core.

Since TIR only occurs at the angle above  $\theta_c$ , maximum number of reflections per unit length,  $N_{max}$  can be computed in terms of index of refraction of fibre in the equation below:

$$N_{max} = \frac{\tan \theta_z}{2r_o} = \frac{\tan \left\{ 90^\circ - \left( \sin^{-1} \frac{n_{clad}}{n_{core}} \right) \right\}_z}{2r_o} \quad (2.22)$$

Where  $\theta_z$  is the angle of ray with respect to z-axis.

## 2.6 Optical Sensor Development and Design

Tracepro<sup>®</sup> (Lambda Research Corporation, U.S.A.) is a useful and flexible optical simulation software in building geometrical models to simulate the scattering and diffraction of light beam and sample the distribution of light. The simulation is designed simply by defining properties for materials and surface desired define Ray tracing point as grid source modelled based on the desired experiment. Figure 2.4 shows the simulation results for the distribution of flux of a circular Gaussian beam directly which is obtained from the light source.

The software simulator would be used to develop an analytical model to empirically study the field distribution of total flux output and number of incident rays. It includes optical properties such as absorption and scattering coefficient; thus, it could be used to model the real experiment.

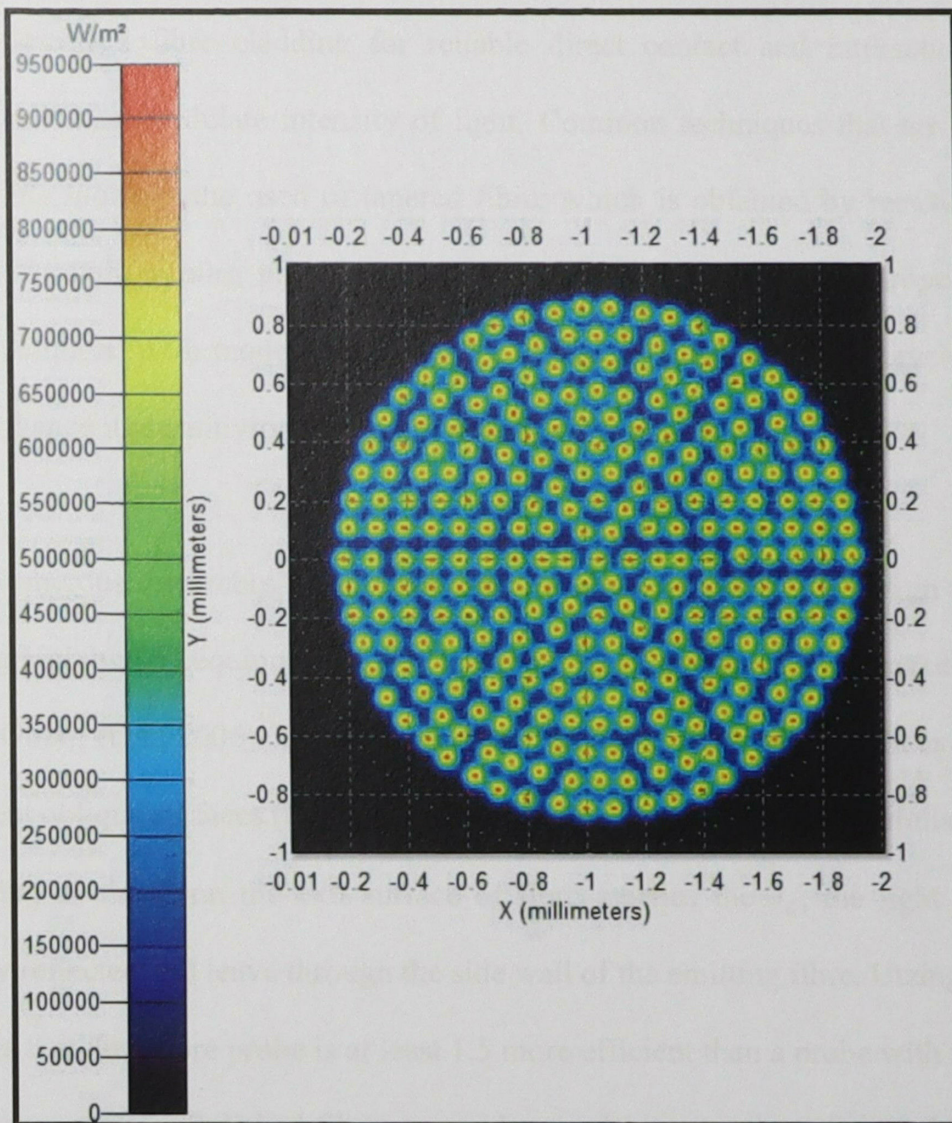


Figure 2.4 Irradiance map displays show irradiance incident on the selected surface in watts per unit area and area in XY axis with millimeters scale.

## 2.7 Application of Evanescent Wave Optic Sensors

In analytical laboratory, fibre optic sensing method is widely used as the tool for determination of physical variables such as concentration, temperature, refractive index and displacement (Alvarado et al., 2014; Chong et al., 2013; Yu et al., 2008). The interaction of the evanescent field of the monochromatic light propagating in the fibre is very sensitive to changes in the surroundings, thus made it useful for sensing. Optical fibre bundles are also used in many sensor applications with removed or

partially removed fibre cladding for reliable direct contact and interaction with external media to modulate intensity of light. Common techniques that are proved reproducible includes the used of tapered fibre; which is obtained by removing the cladding through etching process to allow measurement of optical properties in aqueous solution. With modern heat tapering machine, microfibers are developed to further enhance its sensitivity to external medium (Ji et al., 2012)

Numerous researches were performed for hands on and simple design without involving high budget equipment by mechanically polishing the fibre to make bundle sensors (Oberg et al., 2006). Utzinger reviewed the detection of output light as a result of different oblique surfaces (Utzinger and Richards-Kortum, 2003). He simulated and proved that as the  $\theta_i$  on the exit surface of fibre reaches the  $\theta_c$ , the light is total internally reflected and leave through the side wall of the emitting fibre. Utzinger also concludes that dual fibre probe is at least 1.5 more efficient than a probe with flat tips for sensing purposes. Polished fibres were also used in water detection (Sohn et al., 2002)

Contribution of EW in the design of fibre probe based on absorption and fluorescence sensing operation for monitoring different parameters were inspected. The evanescent optical field detection of the EW interference due to internal incident and refracted rays was demonstrated by Tao et al. (2004). Theoretical studies on wave propagation of side by side fibres based on evanescence have also been reported (Clark and Burrell, 1989; Li and Lit, 1986; Murakami and Sudo, 1981; Reif et al., 2007; Utzinger and Richards-Kortum, 2003). Light rays coupled into the fibre core within a maximum angle with respect to the axis of the fibre core totally reflects at the interface